SCATTERING OF SOUND BY ATMOSPHERIC TURBULENCE: PREDICTIONS IN A REFRACTIVE SHADOW ZONE

Walton E. McBride
Planning Systems, Inc.
Slidell, LA 70458

Henry E. Bass, Richard Raspet, and Kenneth E. Gilbert
University of Mississippi
University, MS 38677

ABSTRACT

According to ray theory, regions exist in an upward refracting atmosphere where no sound should be present. Experiments show, however, that appreciable sound levels penetrate these so-called shadow zones. Two mechanisms contribute to sound in the shadow zone: diffraction and turbulent scattering of sound. Diffractive effects can be pronounced at lower frequencies but are small at high frequencies. In the short wavelength limit, then, scattering due to turbulence should be the predominant mechanism involved in producing the sound levels measured in shadow zones. No existing analytical method includes turbulence effects in the prediction of sound pressure levels in upward refractive shadow zones. In order to obtain quantitative average sound pressure level predictions, a numerical simulation of the effect of atmospheric turbulence on sound propagation is performed. The simulation is based on scattering from randomly distributed scattering centers ("turbules"). Sound pressure levels are computed for many realizations of a turbulent atmosphere. Predictions from the numerical simulation are compared with existing theories and experimental data.

INTRODUCTION

Solar heating of the ground produces strong temperature gradients in the air just above the surface of the Earth. Since the speed of sound is proportional to the square root of the temperature, sound will follow upwardly curved paths in every direction from a source. The stronger the temperature gradients involved, the shorter the distance to what is properly called a shadow zone, since no direct or reflected rays can penetrate into this region. Figure 1 is an illustration of an upward refractive shadow zone where the source is at a height h_s and the radius of curvature of the limiting ray is R_c. The edge of the shadow zone is delineated by the so-called limiting ray which grazes the ground.

In a similar fashion, sound traveling upwind is curved upwards due to the strong wind gradients near the ground and a shadow zone is also formed. In the case of wind, however, the effect is not isotropic because of the vector nature of the wind velocity and the rays are actually bent downward for the sound propagating downwind.

Two mechanisms contribute to the magnitude of the sound levels measured in shadow zones: diffraction and the turbulent scattering of sound. Pierce[1] describes the solution for a linear sound speed

gradient in terms of residue series for the pressure in the shadow zone. He examines the cases of a hard boundary and a pressure-release surface and gives approximate solutions when the source and receiver are above the creeping wave layer height, defined as $(R_c/2\ k_0^2)^{1/3}$, where R_c is the radius of curvature of the limiting ray and k_0 is the wavenumber.

Daigle et al.[2] made use of the above two approximate solutions in an effort to fit the data they collected over an asphalt airport runway and over a grass-covered strip near the runway, the latter approximating a pressure-release surface at frequencies greater than 500 Hz and the former approximating a hard boundary. They found that the hard boundary data was well explained by Pierce's approximate solution for that case and that the data up to 1000 Hz over the grass-covered ground was satisfactorily explained by Pierce's approximate solution for a pressure-release surface.

The approximate solution leads to large errors in the effective source levels for sources close to a pressure-release or finite impedance ground, as was the case with Daigle's data. A complete discussion of this problem can be found in the paper by Raspet and Franke.[3] In a later paper, Berry and Daigle[4] used the complete residue series solution and again compared the above data. They found that the data at 250 Hz still agreed well with the predictions of diffraction theory. But the data was well under-predicted by diffraction theory at 500 Hz and especially at 1000 Hz. The predictions from the full residue series solution are shown in Fig. 2, which is a reproduction of Fig. 13b of Ref. 4.

The role played by atmospheric turbulence in the insonification of shadow zones has escaped analytical formulation. In an effort to obtain a quantitative estimate of the extent to which atmospheric turbulence raises the sound levels in a shadow zone, Gilbert et al.[5] used a parabolic equation method to numerically simulate sound propagation in a turbulent atmosphere. They compared their predictions for upward refracting conditions with experimental results of Wiener and Keast.[6] The numerical predictions involved the calculation of the sound pressure magnitude for a particular realization or "snapshot" of turbulence, while the results of Wiener and Keast were expressed in terms of average sound pressure levels. Nevertheless, Gilbert et al. were able to duplicate the apparent range independence of excess attenuation characteristic of the experimental data at ranges as great as 1 km.

In this paper, we present the average sound pressure levels in an upward refractive shadow zone predicted by a scattering center based numerical simulation. The main features of the numerical solution are reviewed and the modifications necessary to adapt it to an upward refractive atmosphere are discussed. Sound levels are computed for over 500 realizations of the turbulent atmosphere. Predictions from the numerical simulation are then compared with experimental data taken by Daigle et al.[2]

MAIN FEATURES OF THE NUMERICAL SIMULATION

Although the details of the numerical simulation were given in an earlier paper,* the main features are repeated here so that the reader may have a better idea of the type of calculations involved. Following the model of de Wolf,[7] we construct an ensemble of isotropic, irrotational scattering centers which we call "turbules." If μ is defined as the change from unity of the index of refraction, a given turbule is assigned the refractive profile

*Walton E. McBride, Henry E. Bass, Richard Raspet, Kenneth E. Gilbert, "Scattering of sound by atmospheric turbulence," submitted to J. Acoust. Soc. Am., Feb. 1990.

$$\mu(r,s) = q_i\, e^{-r^2/s^2} \tag{1}$$

where q_i is the value of μ at the center of the spherically symmetric turbule and s is the $1/e$ contour of the scattering center and can be considered to be its effective size. The value of q_i and the probability distribution of turbule sizes depend in general on the particular functional form chosen for the correlation function of the fluctuations of the index of refraction. If the correlation function is chosen to have the Gaussian form,

$$\langle \mu_1 \mu_2 \rangle = \left\langle \mu^2 \right\rangle e^{-r^2/L^2}, \tag{2}$$

where $<\mu^2>$ is the variance and L is the correlation length, then the size spectrum is a delta function implying that all the turbules have the same size,

$$s = \frac{L}{\sqrt{2}}\,. \tag{3}$$

The value of q_i for this particular form of the correlation function is given by

$$q_i = \pm \left[\frac{8 \left\langle \mu^2 \right\rangle}{\pi \sqrt{\pi} \rho_N L^3} \right]^{1/2} \tag{4}$$

and is inversely proportional to the turbule number density ρ_N. An upper value of ρ_N of about half the overlap density is necessary so that the turbules will be separate entities. With single scattering, sound scattered from a particular turbule reaches the receiver downfield with negligible scattering by other turbules located between that particular turbule and the receiver. From Eq. (4) the product $q_i^2 \rho_N$ is a constant whose value depends on the independently measured micrometeorological variables $<\mu^2>$ and L. There is, therefore, a certain latitude in the value of ρ_N. Decreasing ρ_N will result in a greater value for $|q_i|$. Although a lesser number of turbules result from a decrease of ρ_N, the predictions of the numerical simulation are statistically steady as the turbule number density is decreased from an upper limit of half the overlap density.

Initially in the development of the simulation, the first Born approximation to scattering was used to determine the scattering effect of each turbule. In practice, the evaluation of the scattering integral is performed by assuming that both source and receiver are far away from the scattering region; thus first order terms in the phase are sufficient. Because some of the turbules in the numerical simulation are close to the source or receiver, second order terms in the phase were kept in the scattering integral. The total pressure at a receiver downfield is, then, the sum of the direct and scattered spherical waves. For only one turbule in free space, this is:

$$p(R) = \frac{e^{ikR}}{R} + \sqrt{\frac{\pi}{2}}\, q_i\, k^2\, s^3\, \frac{e^{ik(r_{st}+r_{tr})}}{r_{st} r_{tr}} \left(\frac{1}{1-ia}\right) e^{-Ck^2 s^2/4}, \tag{5}$$

where

$$C = \left(1-\cos\Theta_0\right)^2 + \sin^2\Theta_0 \left(\frac{1}{1-ia}\right), \tag{6}$$

and

$$a = \frac{ks^2}{2}\left(\frac{1}{r_{st}} + \frac{1}{r_{tr}}\right). \tag{7}$$

In the above equation, k is the wavenumber, s is the effective size of the turbule, Θ_0 is the angle between the incident and scattered directions, R is the distance between source and receiver, while r_{st} is the distance between source and turbule center, and r_{tr} is the distance between turbule center and receiver.

Note that the usual Born scattering term is recovered when a = 0 and the first term in Eq. (6) is dropped. Even with this improved evaluation of the Born scattering integral, the distance from turbule to source or receiver cannot be less than about twice the radius of the turbule. Consequently, "buffers" of a turbule's diameter were placed in front of the source and receiver where no turbules were allowed.

The numerical simulation using the first Born approximation to scattering was then compared to theoretical expressions due to Karavainikov[8] for the log-amplitude and phase variances of the pressure fluctuations. It was found that good agreement was reached whenever the wave parameter D (=R/kL^2) was greater than 1. As shown in Fig. 3, the log-amplitude variances as predicted by Karavainikov are independent of frequency when D < 1, a result also obtained by Bergmann using geometrical optics.

In an effort to reach better agreement in the geometrical optics region, the Rytov approximation used by Karavainikov was incorporated into the numerical simulation. The Rytov method consists of approximating the field at the receiver by

$$\vec{p}^{R}(\vec{r}) = \vec{p}_0(\vec{r})\, e^{\vec{\Psi}^{R}(\vec{r})}; \tag{8}$$

whereas the Born approximation is written:

$$\vec{p}^{B}(\vec{r}) = \vec{p}_0(\vec{r}) + \vec{\Psi}^{B}(\vec{r}). \tag{9}$$

There is a simple relationship between the first Rytov and first Born approximations:

$$\vec{\psi}^{R}_1(\vec{r}) = \frac{\vec{\Psi}^{B}_1(\vec{r})}{\vec{p}_0(\vec{r})}, \tag{10}$$

and it was, therefore, a simple matter to incorporate the first Rytov approximation into the numerical

simulation. The results are shown in Fig. 4 and good agreement is obtained throughout the range of the wave parameter D.

As can be seen from the above comparisons with Karavainikov's analytic curves, the first Rytov approximation is superior to the first Born approximation for an unbounded medium without refraction. When refractive conditions are introduced, however, the formation of shadow zones becomes possible. In the shadow zones, p_0 is 0 and the first Rytov approximation cannot be used. Recourse must be made to the first Born approximation and the wave parameter D must be greater than 1 for the numerical simulation to be valid in accordance with the results of Fig. 3.

The next step is the inclusion of the ground. An immediate consequence of the existence of a boundary is the presence of three additional paths by which sound can propagate to the receiver. There now exist four single scatter paths that connect the source and receiver:

1. source-turbule-receiver,
2. source-turbule-ground-receiver,
3. source-ground-turbule-receiver,
4. source-ground-turbule-ground-receiver.

The last three paths all interact with the ground and, therefore, a model of the effect of the ground on the sound wave was also included in the numerical simulation.

The algorithm proceeds as follows. Values of $<\mu^2>$ and L are given from independent micro-meteorological measurements. From these, the value of s and q_i are obtained using the above equations. A scattering space, which will enclose thousands of turbules, is defined with buffers in front of the source and receivers of widths equal to about the diameter of a turbule. The turbules are assigned positive or negative signs for their value of q_i. The sound pressure at the receiver is calculated for this particular arrangement of turbules, and the result is referred to as a realization. Then each turbule is given random, small increments in its Cartesian coordinates. The sound pressure at the receiver is recalculated, resulting in another realization. The process is repeated for as many realizations as are necessary for the statistics to stabilize. We have found that 500 realizations are sufficient. Average sound pressure levels can then be obtained from the 500 stored values of the sound pressure. It should be mentioned that any other desired statistical quantity can be obtained, such as structure and correlation functions, as well as the variances of the log-amplitude and phase fluctuations.

The inclusion of a sound speed gradient requires two modifications: the rays are now curved and the value of the wavenumber k is no longer constant along a ray. In order to obtain a closed form solution for the equation describing the rays, a linear sound speed gradient was assumed. As is well known, a consequence of this assumption is that the ray paths are arcs of circles.

Because of the curvature of the ray paths, each path must be tested to see whether the source and each turbule can be joined together, as well as each turbule and the receiver. If either segment of the total path cannot be linked, that particular turbule's contribution is discarded. It was found that about 15% of the turbules were eliminated in this way for the experimental data to be described later.

The last correction necessary is the calculation of an effective wavenumber k_e for each ray path. This required the computation of the length of each path, as well as the travel time along that path. Their

ratio gave an effective sound speed c_e along that path, and the effective wavenumber was then given by ω/c_e.

COMPARISON TO DATA

In order to implement the numerical simulation, the statistical properties $<\mu^2>$ and L of the turbulent atmosphere and the impedance of the ground are required. The former was given in the article by Daigle et al.[2] as $<\mu^2> = 6 \times 10^{-6}$ and L = 1.6 m. The impedance had to be approximated because the article mentioned above did not specify a particular impedance model. To estimate the impedance, a residue series solution developed by Raspet and Franke[3] was used to match the curves of Fig. 2 as closely as possible at all three frequencies. The particular impedance model used was a four parameter model developed by Attenborough.[9] A shape factor n' of .750, a shape factor ratio s_f of .875, a porosity Ω of .675, and a flow resistivity σ of 330 cgs rayls give the results shown in Fig. 5.

The numerical simulation was performed with the above parameter values for 500 realizations. Rms sound pressure values were computed and divided by the pressure doubling plus attenuation factor $(2e^{-\alpha R}/R)$ as was done in Daigle's presentation of his experimental data. The source was given a height of 0 m, and six receiver positions were used 230 m downrange at heights of 0.25 m, 0.50 m, 1.0 m, 2.0 m, 4.0 m, and 7.0 m in order to sample the vertical behavior of the sound pressure levels in the shadow zone. Because we are forced to use the first Born approximation when the receiver is in a shadow zone ($p_0 = 0$), the possible values of the wave parameter D must be checked to see that they will be greater than 1. Since $D = R/kL^2$ with R = 230 m and L = 1.6 m, it is sufficient to check the value of D for the greatest frequency of interest. With 1000 Hz, $k \approx 18.4$ and, therefore, $D \approx 5$ which is well above the minimum value of 1. The sound pressure levels predicted by the numerical simulation (expressed in dB) are compared to Daigle's experimental data in Fig. 6 for the three frequencies involved. Notice the similarity in shape which the curves representing the turbulent scattering contribution share with the curves that are typical of diffraction theory predictions. As can be seen by comparing Figs. 2 and 6, it appears that for this experiment the contributions from turbulent scattering and diffractive effects are about equal at 250 Hz. However, turbulent scattering becomes the major contributor at 500 Hz. At 1000 Hz, turbulent scattering is the predominant mechanism behind the increased sound pressure levels measured in the shadow zone.

CONCLUSION

Quantitative predictions for the average sound pressure levels in a refractive shadow zone have been presented. Good agreement was reached with experimental data collected by Daigle et al[2] in a shadow zone caused by temperature gradients. It seems that the use of a simple linear sound speed gradient is a good approximation to the real sound speed profile directly above the ground for the moderate ranges involved in this study. At the longer ranges investigated by Gilbert et al. it was necessary to use a logarithmic sound velocity profile to obtain accurate predictions.[5] The relative contributions of diffraction and turbulent scattering have been examined and graphically displayed. The dominant mechanism which dictates sound levels in shadow zones at higher frequencies is scattering due to turbulence.

ACKNOWLEDGMENTS

This work was supported in part by the Army Research Office. In addition, one of us (WEM) gratefully acknowledges support by the U.S. Army Construction Engineering Research Laboratory.

REFERENCES

1. A.D. Pierce, Acoustics: An Introduction to its Physical Principles and Applications, (McGraw-Hill, New York, 1981).

2. G.A. Daigle, T.F.W. Embleton, and J.E. Piercy, "Propagation of Sound in the Presence of Gradients and Turbulence Near the Ground," J. Acoust. Soc. Am. 79, 613-627 (1986).

3. R. Raspet and S.J. Franke, "Residue Series Solution of Impulse Noise Propagation into a Shadow Zone," J. Acoust. Soc. Am. 83, 1964-1967 (1988).

4. A. Berry and G.A. Daigle, "Controlled Experiments of the Diffraction of Sound by a Curved Surface," J. Acoust. Soc. Am. 83 (6), 2047-2058 (1988).

5. Kenneth E. Gilbert, Richard Raspet, and Xiao Di, "Calculation of Turbulence Effects in an Upward Refracting Atmosphere," J. Acoust. Soc. Am. 87, 2428-2437 (1990).

6. F.M. Wiener and D.N. Keast, "Experimental Study of the Propagation of Sound over Ground," J. Acoust. Soc. Am. 31 (6), 724-733 (1959).

7. D.A. de Wolf, "A Random-motion Model of Fluctuations in a Nearly Transparent Medium," Radio Science 18, 138-142 (1975).

8. V.N. Karavainikov, "Fluctuations of Amplitude and Phase in a Spherical Wave," Akust. Zh. 3, 175-186 (1957).

9. K. Attenborough, "Acoustical Impedance Models for Outdoor Ground Surfaces," J. Sound Vib. 99, 521-543 (1985).

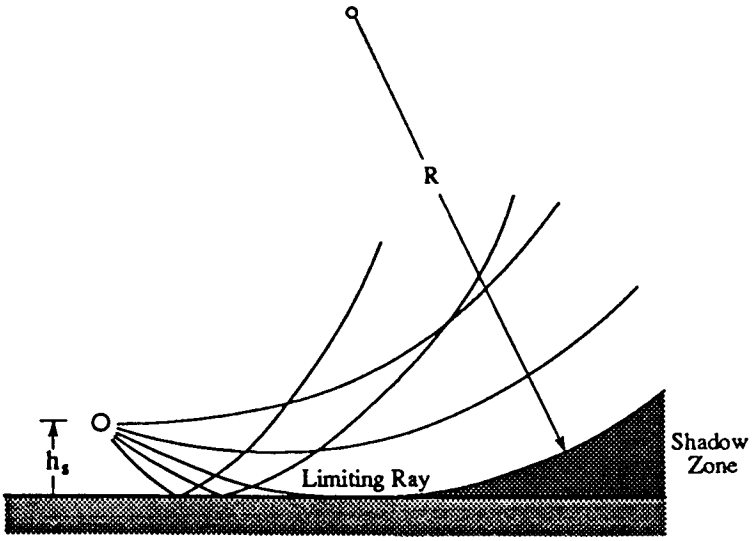

Fig. 1 Shadow zone formation for a sound speed profile that decreases linearly with height.

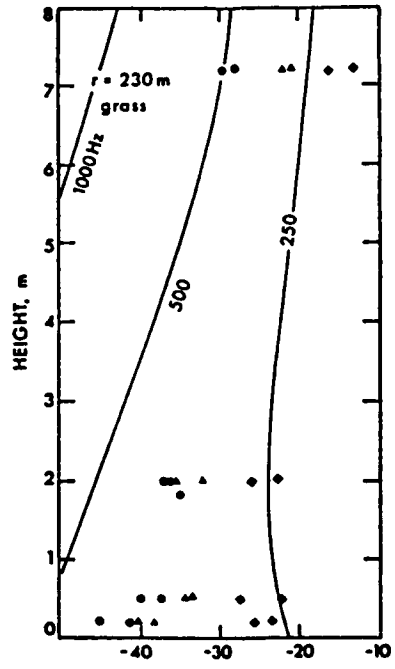

Fig. 2 Comparison of measured sound levels (points) with predictions based upon diffraction into the shadow zone, taken from Ref. 4. Solid circles are for 1000 Hz, triangles for 500 Hz, and diamonds for 250 Hz.

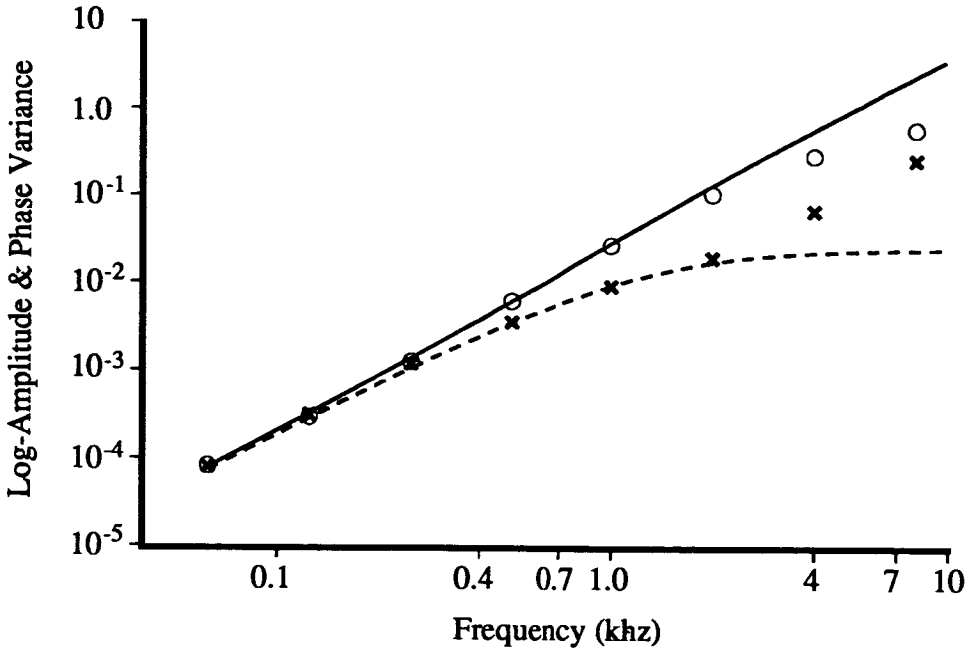

Fig. 3 Comparison of the numerical simulation using the first Born approximation (o for phase variances; x for log-amplitude variances) with Karavainikov's analytical results (——— for phase variances; --------- for log-amplitude variances).

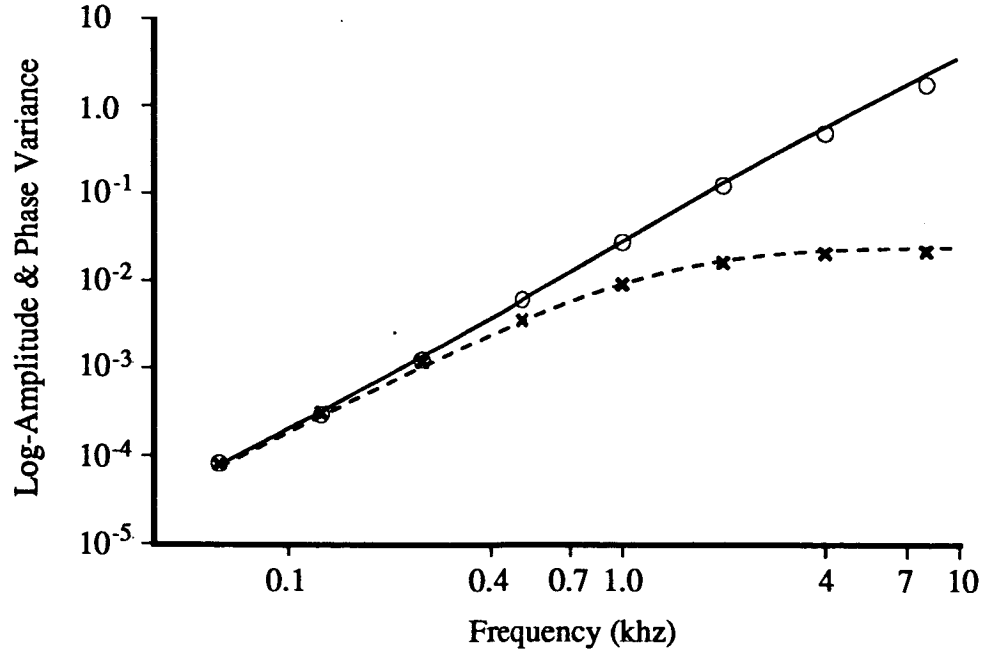

Fig. 4 Comparison of the numerical simulation using the first Rytov approximation (o for phase variances; x for log-amplitude variances) with Karavainikov's analytical results (——— for phase variances; --------- for log-amplitude variances).

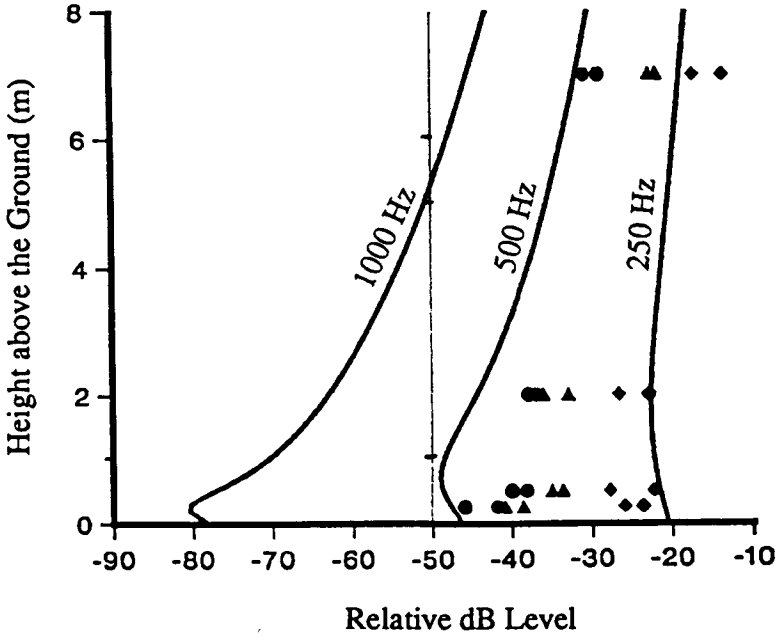

Fig. 5 Comparison of data with the prediction of diffraction theory using the residue series solution. Data points are described for Fig. 2.

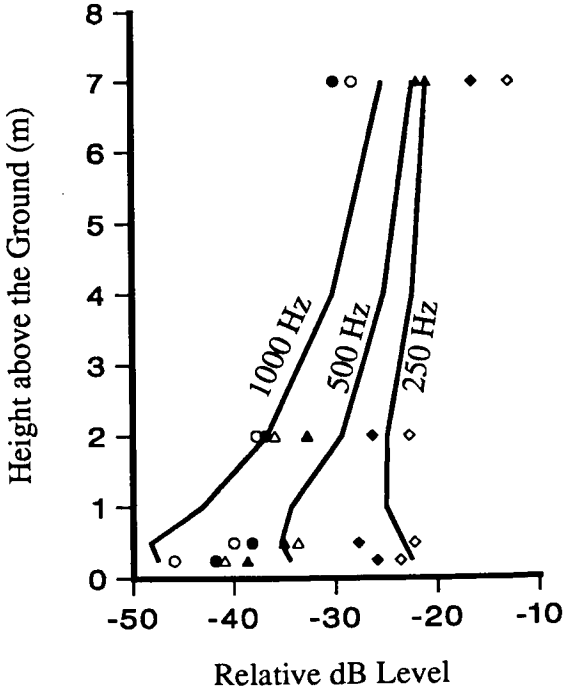

Fig. 6 Comparison of the prediction from the numerical simulation with experimental data taken in shadow zone. Experimental data is the same as in Fig. 5.